

Spike chimera states and firing regularities in neuronal hypernetworks

Cite as: Chaos 29, 053115 (2019); doi: 10.1063/1.5088833

Submitted: 9 January 2019 · Accepted: 24 April 2019 ·

Published Online: 20 May 2019



View Online



Export Citation



CrossMark

Bidesh K. Bera,^{1,2} Sarbendu Rakshit,² Dibakar Ghosh,^{2,a)} and Jürgen Kurths^{3,4}

AFFILIATIONS

¹Department of Mathematics, Indian Institute of Technology Ropar, Punjab 140001, India

²Physics and Applied Mathematics Unit, Indian Statistical Institute, 203 B.T. Road, Kolkata 700108, India

³Potsdam Institute for Climate Impact Research, Potsdam 14473, Germany

⁴Saratov State University, Saratov 4410012, Russia

Note: This paper is part of the Focus Issue, "Nonlinear Chemical Dynamics and Its Interdisciplinary Impact: Dedicated to Ken Showalter on the Occasion of his 70th Birthday".

^{a)}Electronic mail: dibakar@isical.ac.in

ABSTRACT

A complex spatiotemporal pattern with coexisting coherent and incoherent domains in a network of identically coupled oscillators is known as a chimera state. Here, we report the emergence and existence of a novel type of nonstationary chimera pattern in a network of identically coupled Hindmarsh–Rose neuronal oscillators in the presence of synaptic couplings. The development of brain function is mainly dependent on the interneuronal communications via bidirectional electrical gap junctions and unidirectional chemical synapses. In our study, we first consider a network of nonlocally coupled neurons where the interactions occur through chemical synapses. We uncover a new type of spatiotemporal pattern, which we call "spike chimera" induced by the desynchronized spikes of the coupled neurons with the coherent quiescent state. Thereafter, imperfect traveling chimera states emerge in a neuronal hypernetwork (which is characterized by the simultaneous presence of electrical and chemical synapses). Using suitable characterizations, such as local order parameter, strength of incoherence, and velocity profile, the existence of several dynamical states together with chimera states is identified in a wide range of parameter space. We also investigate the robustness of these nonstationary chimera states together with incoherent, coherent, and resting states with respect to initial conditions by using the basin stability measurement. Finally, we extend our study for the effect of firing regularity in the observed states. Interestingly, we find that the coherent motion of the neuronal network promotes the entire system to regular firing.

Published under license by AIP Publishing. <https://doi.org/10.1063/1.5088833>

Several cognitive neuronal processes strictly depend on interneuronal communications that take place mainly through two types of synapses: the electrical communication via gap junctional and the chemical synaptic interaction. Neuronal synchrony plays a fundamental role in the normal operation of various neuronal processes. In particular, this property is closely related to the neuronal plasticity, information exchange, etc. Chimera state is a self-organized complex spatiotemporal pattern that deals with the simultaneous appearance of synchrony and desynchrony behaviors in the neuronal networks. The emergence of the chimera states in the neuronal network was investigated previously by considering the electrical and the chemical synaptic coupling or the interaction through another medium. In all previous studies on chimera states, only bidirectional chemical synaptic interactions were considered. However, in the real situation,

chemical communication happens unidirectionally between two neurons, whereas electrical communication happens bidirectionally between two adjacent neurons. In this context, here, we study the existence and emergence of chimera patterns in a neuronal hypernetwork by taking a unidirectional chemical synapse and bidirectional electrical coupling. In our study, each neuron in the network is modeled with a Hindmarsh–Rose neuronal oscillator. Through the interplay of the network topology and the chemical synaptic coupling function, a novel type of nonstationary chimera pattern, called "spike chimera," is found, which is characterized by uncorrelated spikes and a coherent quiescent state of the coupled neurons. These complex spatiotemporal patterns are robust with respect to initial conditions. We investigate the firing regularities of the coupled neurons in different dynamical states. With the help of various measurements, the different

collective dynamical features, such as incoherent, coherent, steady state dynamics, and spike chimera states, are characterized and quantified in the parameter space.

I. INTRODUCTION

One of the most challenging issues pertaining to the living world is the understanding of neuronal communication in the human brain. The underlying complexity arises due to the presence of a large number of neurons and synapses through which neurons are connected.¹ The interneuronal communication among the neurons happens through the synaptic interactions. Mainly, two types of synapses are identified in neuronal communication, namely, electrical gap junction and chemical synapse. The former type is located between two adjacent membrane potentials of the neurons making the gap junction between the pre- and postsynaptic neurons. The corresponding functional form of this mutual type of interaction is defined as the difference between the membrane potentials. However, the chemical synaptic interaction always takes place unidirectionally, where the signal is conveyed chemically via neurotransmitter molecules through the synapses.² The functional form of this synaptic interaction is considered as a nonlinear sigmoidal input–output function. Through the electrical synapse, calcium, inositol-1,4,5 trisphosphate, and cyclic AMP molecules are transferred bidirectionally, thereby making the gap junction between two adjacent cells, while gamma-aminobutyric acid, acetylcholine, dopamine, and serotonin packages are transferred chemically via chemical synapses inside the synaptic vesicles.³ For the electrical gap junction, the distance between pre- and postsynaptic ends is approximately 3.5 nm, whereas for chemical synapses, these are comparatively large, nearly 20–40 nm.⁴ These two types of synapses exist simultaneously in most of the nervous systems and operate independently.³ The coexistence of two or more interaction functions or coupling topologies in a complex network is called “hypernetwork.”⁵ Here, the simultaneous presence of both synaptic interactions on the neuronal network leads to “neuronal hypernetwork.”⁶

Neuronal rhythmic behavior plays an important role for the normal coordination in several neuronal processes, such as visual information processing, sleeping, and memory in the brain.^{7–9} The rhythmic nature of a large number of interacting neurons does not always appear spontaneously; rather, it may have different forms of oscillatory patterns that include incoherent (disordered/desynchronized) or coherent (ordered/synchronized) motion or the coexistence of both. In the nonlinear dynamics literature, the simultaneous existence of synchronous and asynchronous behavior is known as the “chimera state,”^{10,11} and this has a strong connection to several neuronal processes. A spatially localized pulselike neuronal activity appears due to the recurrent excitations of the spiking neurons.¹² In the case of bump states, the spatially localized region consists of both coherent and incoherent neuronal oscillations in such a way that the fully incoherent region covers the partially coherent area that has a clear resemblance to the chimera state. Apart from this, the unihemispheric slow wave sleep^{13,14} is one of the prominent behavioral phenomena, which is often observed in some aquatic mammals, migratory birds, eared seal, etc. During their sleep time, they unyoke only one part of cerebral hemisphere of the brain by closing the

opposite eye, while the other part of the brain monitors what is happening in the environment. This phenomenon strongly indicates that the neuronal oscillations in the wake part of the brain are desynchronized, whereas in the sleepy part, they are strongly synchronized. This simultaneous coexistence of neuronal activity in the brain is quite similar to Kuramoto’s observation in 2002 that a network of nonlocally coupled identical phase oscillators¹⁰ spontaneously breaks down into coherent and incoherent dynamics for certain interaction strengths and coexist with each other. Such type of dynamics also emerges in coupled dynamical networks in various systems,¹⁵ including ecological systems,¹⁶ chemical systems,^{17,18} optical systems,¹⁹ and neuronal systems.^{20,21} Different types of chimera patterns²² were studied in symmetrically coupled local,^{20,23,24} nonlocal,^{10,11} and global²⁵ networks as well as complex networks.^{26,27} Recent results have identified the emergence of chimera states in modular²⁸ and multiplex²⁹ architectures as well. In Ref. 30, authors presented a method to engineer a chimera state on the edges of a network by an appropriate distribution of heterogeneous time delays. Recently, the impact of repulsive interlayer links on the occurrence of chimera states has been observed in attractive intralayer connections.³¹ Using electrical and chemical synapses, three different topologies of neuronal networks are possible, one of which is constructed by solely the presence of bidirectional electrical synapses, while another one by solely the presence of unidirectional chemical synapses. The third possible type of network is composed of a combination of these two types of synapses, which constitute a neuronal hypernetwork. From a neurobiological point of view, chemical synaptic communication always happens in a unidirectional mode due to the ion polarizing effect, but electrical synaptic communication always takes place in a bidirectional manner through gap junctions and both types of synapses coexist in most of the nervous systems while performing independently. Most of the previous studies^{20,22,32} on chimera states in neuronal networks are concerned with the presence of either solely electrical or solely chemical synapses. So, from a neurobiological perspective, the study of chimera patterns in the presence of both electrical and chemical synapses deserves special attention.

Inspired by the above facts, we systematically study the different collective dynamical features such as incoherent, chimera (coexistence of coherence and incoherence), coherent, and steady states of the coupled neuronal network and also enunciate the transition scenarios among them. Each node of the dynamical network is modeled through the Hindmarsh–Rose neuron, which is known for several bursting dynamical features. First, we investigate the emergence and existence of chimera states in a one way nonlocally coupled neuronal network, where the interaction function is considered as a chemical synaptic function. Using spatiotemporal plot and local order parameter,^{22,33} the existence of chimera states together with coherent, incoherent, and steady states is characterized. Here, our observe chimera states are quite different from the classical chimera states because in the quiescent state, all the coupled neurons follow the coherence profile, whereas chimeras appear only in the spiking states (firing pattern). We designate this type of chimera state as spike chimera. More precisely, the desynchronized spikes together with coherent quiescent states induce these spiking chimera patterns. The existence of such type of chimera states is characterized by the instantaneous strength of incoherence and global order parameter. To distinguish the chimera states from the other dynamical states, such

as incoherent, synchronization, and steady states, the time-average statistical measurement, namely, the strength of incoherence (SI)³⁴ is used. Another significance of the present work is the analysis of the effect of bidirectional electrical gap junctional coupling. It is observed that with the addition of the local bidirectional electric coupling together with the local chemical synaptic interaction, a coupled neuronal network produces traveling type nonstationary chimera patterns. The presence of both local synaptic interactions gives further relaxation for the essential requirement as the nonlocal connectivity for the emergence of chimera states in the network. As such, dynamical features including chimera states have a strong dependence on the initial conditions. So, based on the SI measurement, we quantified all these states in the “basin stability” (BS) framework.^{35,36} This pioneering BS measure is a universal nonlocal nonlinear concept and interplays with a large number of initial conditions from the basin of attraction. Finally, we investigate the firing regularity of each individual neuron corresponding to different collective dynamical states. By calculating two quantities, namely, the interspike interval and the coefficient of variation, the regularity of the firing pattern of the spike train of each neuron in the neuronal network is analyzed.

This paper is organized in the following way. Section II introduces the mathematical framework of the coupled Hindmarsh–Rose neuronal network model, by considering both types of interacting synapses. In Sec. III, by means of numerical simulations, the emergence of spike chimera state is discussed by taking solely unidirectional chemical synapses. Section IV is devoted to the results for neuronal hypernetwork constituted by unidirectional chemical and bidirectional electrical synapses, where imperfect traveling chimera emerges. The coexistence of these nonstationary chimera states with different dynamical states such as incoherent and coherent states is discussed in Sec. V. The different multistable states are quantified and distinguished by BS measurement, time-average SI, and velocity profile. Section VI provides the firing regularities of the individual neurons in the chimera states observed in Secs. III and IV using interspike interval and coefficient of variation. The conclusions of our findings are given in Sec. VII.

II. MATHEMATICAL MODEL FOR A NETWORK OF HINDMARSH-ROSE NEURON

We consider a neuronal network consisting of N identical Hindmarsh–Rose (HR) neurons. Through chemical synapses, the information is conveyed unidirectionally between distantly situated neurons, whereas electrical synapses are bidirectional in nature and can transfer signal only among neighboring neurons. So, from this physical relevance of synaptic communication processes, we regard the chemical synaptic interaction as unidirectional in a nonlocal fashion and bidirectional local electrical coupling. Considering the prescribed interactions in the HR neuronal network, the evolution equation of the i th neuron is given by

$$\begin{aligned} \dot{x}_i &= y_i - ax_i^3 + bx_i^2 - z_i + I + \frac{g_c}{k_c}(v_s - x_i) \sum_{j=i+1}^{i+k_c} \Gamma(x_j) \\ &\quad + \epsilon(x_{i+1} + x_{i-1} - 2x_i), \\ \dot{y}_i &= c - dx_i^2 - y_i, \\ \dot{z}_i &= \mu(s(x_i - x_0) - z_i), \quad i = 1, 2, \dots, N. \end{aligned} \quad (1)$$

Here, N is the total number of neurons in the coupled network and k_c denotes the number of neurons coupled with the nearest neighbor in a one way (unidirectional) ring with the coupling radius $R = \frac{k_c}{N}$. The variable x_i denotes the membrane potential of the i th HR neuron and the other variables y_i and z_i are associated with the transport of ions across the membrane. y_i represents the fast channel (associated with Na^+ or K^+) and z_i corresponds to the slow current (associated with Ca^{2+}). The modulated value of the parameter μ determines the speed controller corresponding to the slow-fast dynamics. The parameters g_c and ϵ , respectively, denote the chemical synaptic and electrical interaction strengths, which determine how the information is distributed among the neurons through the different types of synaptic interactions. The considered chemical synaptic function is modeled by a sigmoidal input–output nonlinear function, described as $\Gamma(x_i) = \frac{1}{1+e^{-\lambda(x_i-\Theta_s)}}$, where the parameter $\lambda = 10$ determines the slope of the function and $\Theta_s = -0.25$ denotes the synaptic firing threshold. Here, v_s represents the synaptic reversal potential, for $v_s > x_i(t)$ the synaptic current has a depolarizing effect that makes the synapse excitatory, and for $v_s < x_i(t)$, the synaptic current has a hyperpolarizing effect making the synapse inhibitory. Here, I represents the external stimulus control parameter that measures the current that enters in the neuron. We fix the parameter values as $a = 1, b = 3, c = 1, d = 5, \mu = 0.005, s = 4, x_0 = -1.6, I = 3.25$, in which the uncoupled neuron exhibits a square wave bursting dynamics. For the above chosen set of parameter values, the membrane potentials $|x_i(t)| < 2$ ($i = 1, 2, \dots, N$) for all time t . For the choice of fix $v_s = 2$, the term $(v_s - x_i(t))$ in Eq. (1) is always positive. So, the inhibitory and excitatory natures of the synapses depend on the sign of the chemical synaptic coupling strength g_c . In our case, to make the chemical synapse excitatory, we chose $g_c > 0$, i.e., when the presynaptic neuron spikes, it induces the postsynaptic neuron to spike.

A schematic diagram illustrating such a hypernetwork for $N = 8$ nodes (solid green circles) is shown in Fig. 1. The blue solid lines represent the nearest neighbor bidirectional electrical gap junctions and the dashed red lines are nonlocal unidirectional couplings via chemical synaptic transmission with the coupling radius $R = 0.25$ (constant in-degree 2). The coexistence of these two networks constitutes a hypernetwork, where each layer representing a different kind of interaction. In our numerical simulations, we consider a neuronal network of size $N = 200$. Using the fifth order Runge–Kutta–Fehlberg algorithm, we integrate the coupled system (1) with step size $\Delta t = 0.01$ up to 10^6 time iterations. The initial condition for each oscillator is chosen from the phase space volume. We first concentrate our study on the sole presence of nonlocal unidirectional chemical synaptic coupling. The next combined effect of chemical and electrical synapses on chimera states is discussed.

III. UNIDIRECTIONAL CHEMICAL SYNAPSE

In this section, we study the emergence and existence of chimera patterns in unidirectional coupled neurons through chemical synapses, i.e., for $\epsilon = 0.0$ in Eq. (1). For the fixed coupling radius $R = 0.4$, different types of collective dynamical states appear as illustrated in Fig. 2 by varying the chemical synaptic interaction strength g_c . The snapshots of the amplitudes (membrane potential) of all neurons at a particular instant $t = 2380$ are plotted in the left panel

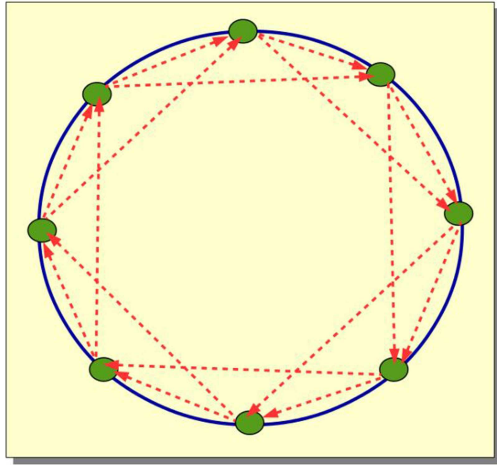


FIG. 1. Schematic diagram of a neuronal hypernetwork. Solid green circles represent HR neurons connected with their nearest neighbors by local gap junction (blue solid lines) and nonlocal chemical synapses (red dashed lines).

of Fig. 2. For the lower coupling strength $g_c = 0.1$, all the neurons are randomly distributed, which signify that they are in an incoherent regime and the snapshot is shown in Fig. 2(a). With increasing the chemical synaptic strength to $g_c = 0.4$, we find that some coherent population is interspersed by one incoherent group, which is a signature of chimera state depicted in Fig. 2(d). Further increased values of $g_c = 1.1$ and $g_c = 1.4$, two structurally different types of fully coherent dynamics appear, one is a synchronized state and the other is steady state (global death) represented in Figs. 2(g) and 2(j), respectively. In the synchronized coherent state, all the neurons are in oscillatory motion and follow a smooth profile [Fig. 2(g)], while for global death, the coherent state [Fig. 2(j)], all the neurons in the network converge to a coupling-dependent nontrivial homogeneous steady state. The fixed points of the coupled system (1) (X_0, X_1, \dots, N -times), $X_0 = (x^*, y^*, z^*)$ are given by the real roots of the equations $ax^{*3} + (d - b)x^{*2} + s(x^* - x_0) - g_c(v_s - x^*)\Gamma(x^*) - (I + c) = 0$, $y^* = c - dx^{*2}$, $z^* = s(x^* - x_0)$.

To see the long-time behavior of the individual neurons, the space-time plots for the different dynamical states corresponding to the left panel are drawn in the middle panel of Fig. 2. In the incoherent state, all the neurons are uncorrelated and randomly distributed over a long time period, shown in Fig. 2(b). For the chimera state, a group of coherent population is divided by an incoherent population for a sufficient long time period ($2300 \leq t \leq 2350$ and $2450 \leq t \leq 2500$), which is a strong indication of the existence of a chimera state on those time periods, described in Fig. 2(e). It is also noted that all the neurons follow a coherent motion during the time period $2350 < t < 2450$. This type of scenario occurs due to the presence of a multitime scale dynamics in the individual nodes. In the coherent time duration, all the neurons are in the quiescent states and have phase coherence, whereas in the other two time intervals, few or all the neurons are in different types of spiking dynamics, which yield the appearance of chimera states. Hence, this chimera state is not

static in time; rather, it oscillates with the coherent state according to the spiking and bursting dynamics of each neuron. This fact inspires us to entitle the new type of chimera pattern as spike chimera. Upon increasing the synaptic coupling strength to $g_c = 1.1$, all the neurons are in phase coherence [corresponding to Fig. 2(g)] irrespective of the time evolution of each neuron (spiking and bursting), which is clearly shown in Fig. 2(h). For higher values of the chemical synaptic strength at $g_c = 1.4$, all the neurons are settled down in resting states, which mean they are all converged to the coupling dependent fixed point (x^*, y^*, z^*) , i.e., the global death state. This feature is delineated in Fig. 2(k). The transition from oscillatory to steady state dynamics has a great relevance in neuroscience where the neuronal output can be controlled by using this chemical synaptic coupling. So, it is clear that the chimera patterns are not static in time, rather they are time-varying, which signify the emergence of the nonstationary chimera patterns in the neuronal network.

To characterize the spatial coherence-incoherence patterns in the chimera state, we adopt the notion of “local order parameter.”²² This real-valued quantity actually signifies the neighbor ordering of the neurons in the network and is defined as

$$L_i = \left| \frac{1}{2\gamma} \sum_{|i-k| \leq \gamma} e^{i\phi_k(t)} \right|, \quad (2)$$

where $j = \sqrt{-1}$, $i = 1, 2, \dots, N$, and γ denotes the window size of the i th neuron, which is used for the spatial average. The geometric phase of the i th neuron at time t is defined as $\phi_i(t) = \tan^{-1} \frac{y_i(t)}{x_i(t)}$, which is a good approximation for $\mu \ll 1$. The local order parameter value $L_i = 1$ represents the maximum coherency of the i th neuron and indicates that the i th neuron belongs to the coherent population of the chimera state. On the other hand, a value of L_i less than 1 signifies the incoherent position of the i th neuron. To characterize the coexistence of coherent and incoherent patterns, we plot the local order parameter in the right panel of Fig. 2 corresponding to the left panel where the color bars represent the variation of the local ordering of the neurons. Deep red and blue regions denote the coherent and incoherent states, respectively. From Fig. 2(f), it is also clear that during the time period $2350 < t < 2450$, all the neurons are in maximum coherency due to the quiescent state.

So, our observed chimera pattern differs clearly from the classical chimera states; it is a new type of nonstationary chimera state, which we call spike chimera. This chimera pattern has a temporal variation in the sense that it appears for spikes only, while the quiescent state always follows phase coherence. To characterize such chimera states, we plot the time evolution of all the neurons in the network in Fig. 3(a) and calculate the instantaneous strength of incoherence $SI(t)$ [Fig. 3(b)] and order parameter $\rho(t)$ [Eq. (5); Fig. 3(c)]. To calculate $SI(t)$, we divide the total number of neurons in the network into M even number of bins, each of which in the equal length $n = \frac{N}{M}$. Then, we introduce the instantaneous local standard deviation $\sigma(m, t)$, which is defined as

$$\sigma(m, t) = \sqrt{\frac{1}{N} \sum_{j=n(m-1)+1}^{mn} (w_j - \langle w \rangle)^2}, \quad (3)$$

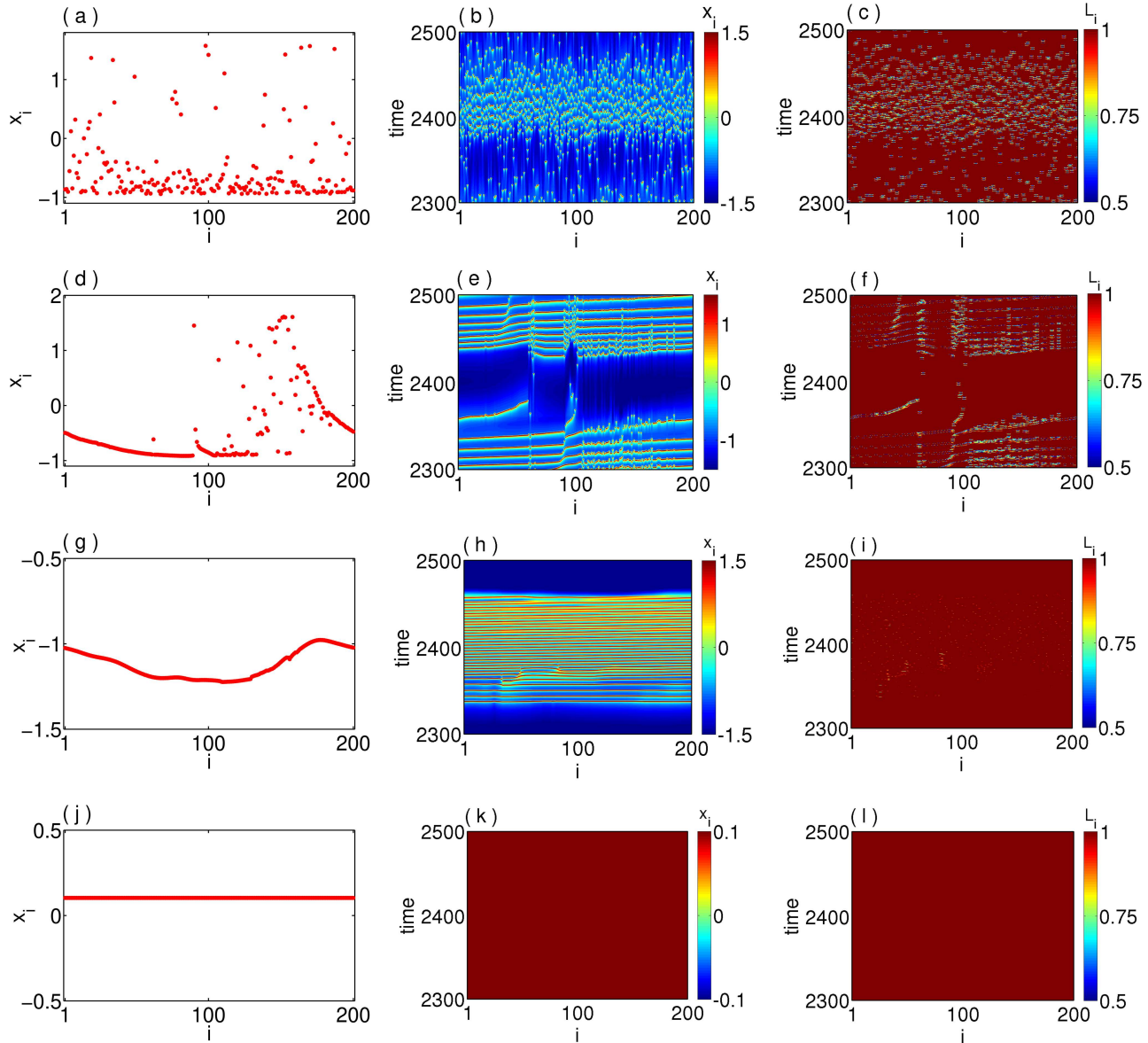


FIG. 2. Snapshot of amplitude of the membrane potential x_i (left panel), spatiotemporal plot of x_i (middle panel), and long term variation of the local order parameter L_i (right panel), with index i for the incoherent state where $g_c = 0.1$ (first row), chimera state, $g_c = 0.4$ (second row), synchronous coherent state, $g_c = 1.1$ (third row), and coherence death state, $g_c = 1.4$ (fourth row). Coupling radius is fixed at $R = 0.4$.

for $m = 1, \dots, M$. Here, $w_i(t)$ be the difference of the potential variables, defined as $w_i(t) = x_i(t) - x_{i+1}(t)$, $i = 1, 2, \dots, N$, with the boundary condition $x_{N+1}(t) = x_1(t)$. This difference variable represents the local coherence of the neighboring neurons, which means that if two neighbor neurons are in a coherent state, then $w_i \rightarrow 0$ and for an incoherent state, w_i takes a nonzero value. $\langle w \rangle = \frac{1}{N} \sum_{i=1}^N w_i(t)$, and $\langle \cdot \rangle_t$ denotes the time average. The instantaneous strength of

incoherence $SI(t)$ is defined as

$$SI(t) = 1 - \frac{1}{M} \sum_{m=1}^M \Theta(\delta - \sigma(m, t)), \quad (4)$$

where $\Theta(\cdot)$ is the Heaviside step function and δ is the predefined threshold; here, we choose $\delta = 0.16$. Consequently, $SI(t) = 1$ and

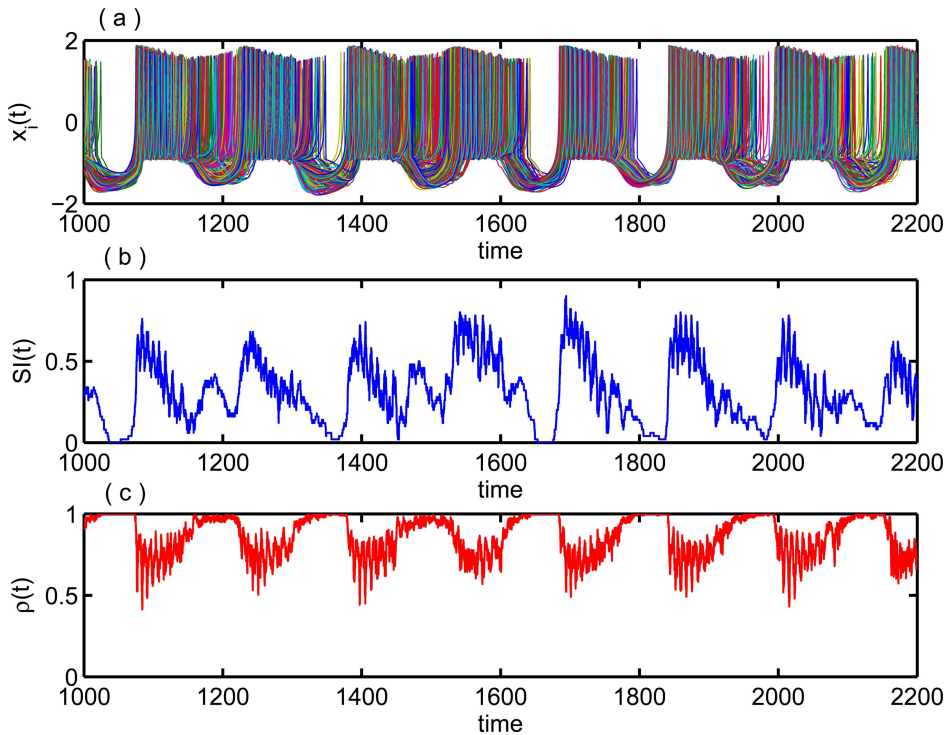


FIG. 3. (a) Time evolution of x_i for the spike chimera state is plotted for $g_c = 0.4$. Variation of the instantaneous (b) strength of incoherence $SI(t)$ and (c) order parameter $\rho(t)$ with respect to time.

$SI(t) = 0$ represent the incoherent and coherent states, respectively, at instant time t , while $0 < SI(t) < 1$ represents the chimera state. Next, we define the order parameter $\rho(t)$ as

$$\rho(t) = \left| \frac{1}{N} \sum_{j=1}^N e^{i\phi_j(t)} \right| \quad (5)$$

to compute the spontaneous synchronization level of the neural activity within the network. $\rho(t) = 1$ corresponds to complete synchronous activity at time t , whereas $\rho(t) = 0$ represents a desynchronization state. The variations of $SI(t)$ and $\rho(t)$ with respect to time are shown in Figs. 3(b) and 3(c), respectively. From Fig. 3(b), it is observed that the $SI(t)$ fluctuates in $[0, 1]$ and is 0 at the quiescent state and $SI(t) \in (0, 1)$ for the spiking state, which means that all the quiescent states follow the coherent motion and the spiking time represents the chimera state. To clearly characterize this scenario, we plot a variation of $\rho(t)$ in Fig. 3(c), where $\rho(t) = 1$ for the coherent state and $\rho(t) \in (0, 1)$ for the chimera state. Figure 4 shows the snapshots at four different time instants for chimera and coherent states to verify the above scenario. The snapshots at time $t = 1040$ and $t = 1668$, and the phase coherence at quiescent states are shown, respectively, in Figs. 4(a) and 4(d). Due to spiking, the spatial coexistence of coherent and incoherent states is observed in Figs. 4(b) and 4(c), where the snapshots are taken at $t = 1200$ and $t = 1495$, respectively. So, from Figs. 3 and 4, it is noticeable that the simultaneous appearance of the quiescent state of all neurons always maintains a phase coherence, while the spiking of the neurons is responsible for the chimera state.

Consequently, the chimera state does not persist in the entire time span, rather it can only be observed in the spiking time.

Next, to distinguish the incoherent, spike chimera, and coherent states, we use a time-average statistical measurement as the strength of incoherence,

$$SI = \langle SI(t) \rangle_t. \quad (6)$$

Here, we characterize a dynamical state as incoherent if its dynamics remain desynchronized for all time t [i.e., $SI(t) = 1, \forall t$] and the coherent state if it is in a phase coherent state for any time instance [i.e., $SI(t) = 0, \forall t$]. Therefore, $SI = 1$ and $SI = 0$ represent the incoherent and coherent states, respectively. For spike chimera state, $SI(t) \in [0, 1]$ for all t . When all the neurons in the network are in quiescent state, $SI(t) = 0$. Hence, a long-time average of the strength of incoherence is necessary for characterizing this state which yields $SI \in (0, 1)$.

To distinguish between the two different types of coherent states that we have already observed, one is oscillatory and the other a steady state, we calculate the time-average velocity V of the entire network, which is defined as

$$V = \left\langle \frac{1}{N} \sum_{i=1}^N \sqrt{\dot{x}_i^2 + \dot{y}_i^2 + \dot{z}_i^2} \right\rangle_t. \quad (7)$$

Here, $V = 0$ implies that each oscillator of the entire network converges to a coupling-dependent steady state (x^*, y^*, z^*) . Finally, the values of $SI = 0$ together with nonzero velocity ($V \neq 0$) indicate the synchronized coherent motion, while $SI = 0$ with $V = 0$ signify the coherent steady state.

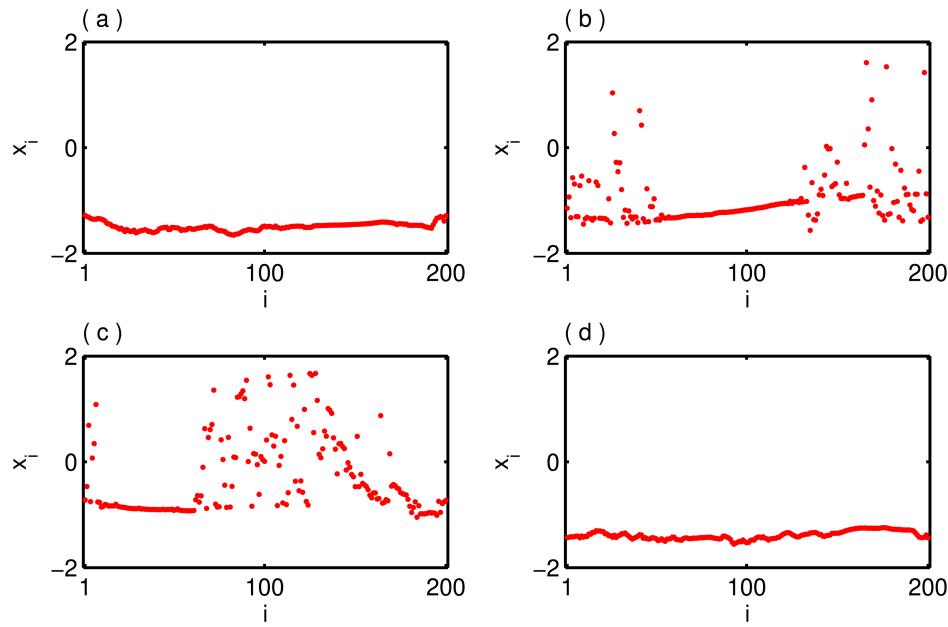


FIG. 4. Snapshot of the amplitudes x_i of all the neurons at (a) $t = 1040$, (b) $t = 1200$, (c) $t = 1495$, and (d) $t = 1668$. Other parameters are the same as in Fig. 3.

For a wide range of chemical synaptic coupling strength g_c and nonlocal coupling radius R , we espy these dynamical states by simultaneously varying these two parameters. Based on the SI measurement, the two-parameter phase diagram in the (R, g_c) plane is drawn in Fig. 5(a) to reveal the complete scenario for the existence of spike chimera together with incoherent and coherent states. Figure 5 shows the two-parameter phase diagram when the uncoupled individual neurons are oscillating chaotically and incoherently, i.e., $g_c = 0$. By introducing the chemical synaptic interaction strength g_c with varying the coupling radius R , the incoherent state persists up to certain values of g_c , which is clearly seen in Fig. 5(a), where $SI = 1$ (denoted by the deep red region). Further increasing of g_c or R , we find that spike chimera states emerge where the value of SI varies between 0 and 1 (other colors except deep red and black). Then, the chimera

state loses its stability and transits into a coherent state. In this state, the value of SI is zero and is marked as black in Fig. 5(a). Here, two structurally different coherent states emanate, one is synchronous oscillation and the other a nontrivial homogeneous steady state. In the latter case, all the neurons converge to a coupling-dependent fixed point. To distinguish these two coherent states, we calculate the velocity V , Eq. (7) in which $V = 0$ corresponds to the steady state coherent dynamics (black region) as shown in Fig. 5(b).

IV. NEURONAL HYPERNETWORK

The chimera pattern of the coupled neuronal network in the presence of both electrical and chemical synapses will be deliberated in this section. The simultaneous presence of the different types

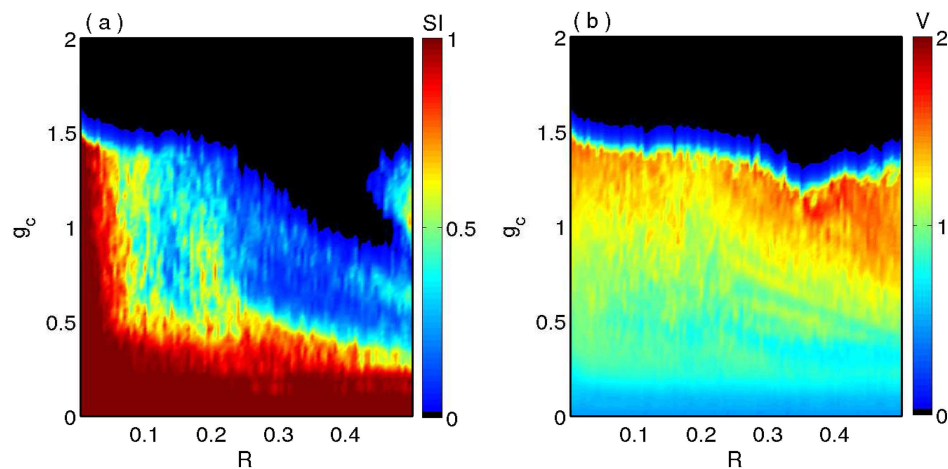


FIG. 5. Two-parameter (R, g_c) phase diagram: variation of (a) strength of incoherence where deep red for incoherent states, black for coherent states, and other colors indicate the existence of chimera states, (b) velocity (V) of the entire network where black represents the region of coherent steady state.

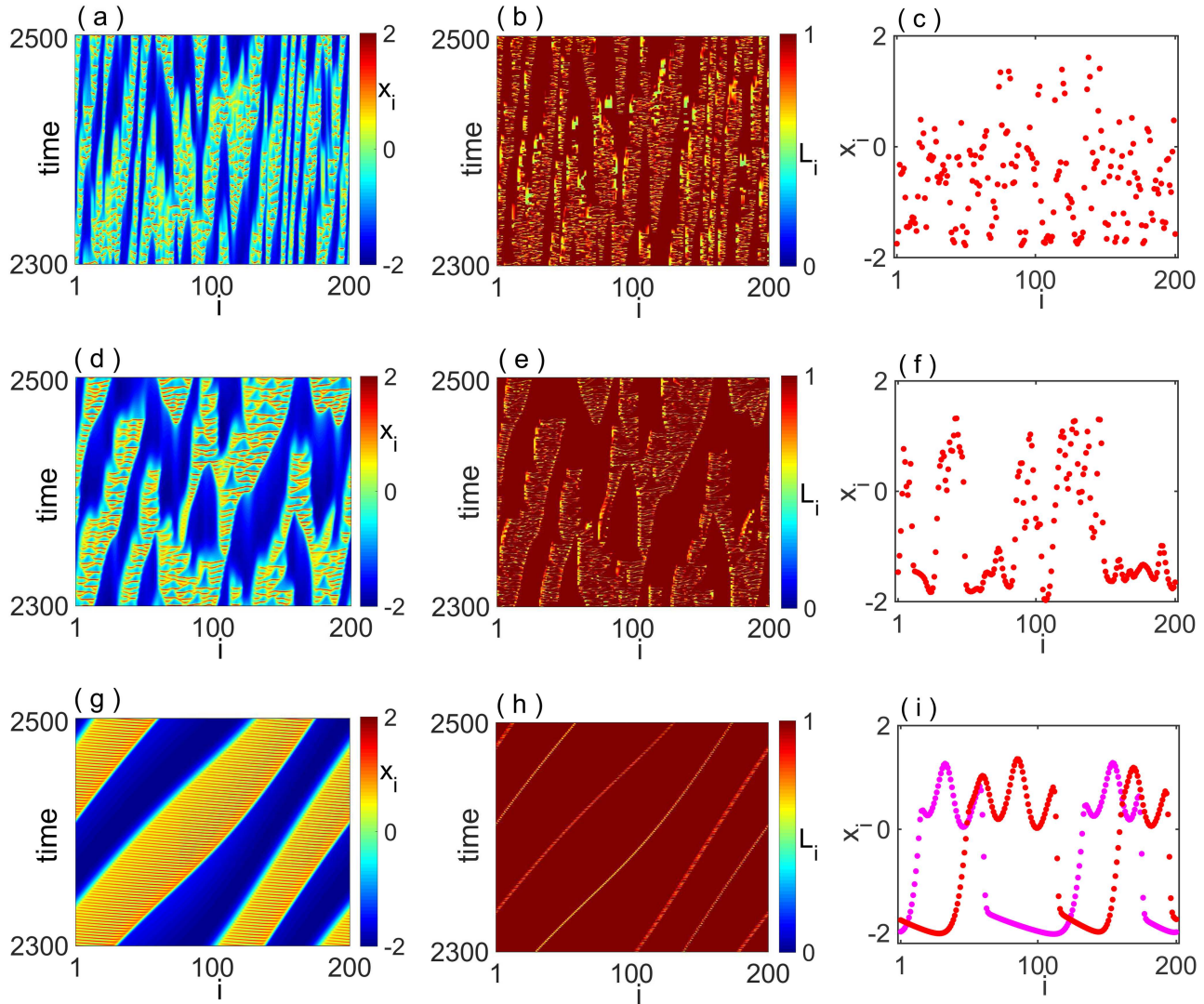


FIG. 6. Hypernetwork with local unidirectional chemical synaptic and local bidirectional electrical coupling. Left panel: spatiotemporal plot, middle panel: local order parameter, and right panel: snapshot of amplitude. (a)–(c) $\epsilon = 0.25$, $g_c = 0.1$, imperfect traveling chimera state; (d)–(f) $\epsilon = 1.5$, $g_c = 0.6$, imperfect traveling chimera state; and (g)–(i) $\epsilon = 4.6$, $g_c = 1.32$, traveling coherent state.

of interaction functions in the network, known as hypernetwork, is one of the most important topics in current complex network research. A neuronal communication is a significant practical example of hypernetwork, as the neurons interact through both electrical gap junctions as well as chemical synapses. We consider neuronal hypernetworks where neurons are connected through the chemical synapses in one way via local and nonlocal topologies with the coupling strength g_c and local bidirectional electrical gap junction with the interaction strength ϵ [cf. Eq. (1)]. In such neuronal hypernetworks, we identify the emergence of imperfect traveling chimera states for local chemical and electrical coupling. Previously, such type

of chimera patterns was observed in a nonlocally coupled Kuramoto model³⁷ in the presence of inertia term. As expected for lower synaptic coupling strengths, we found incoherent states (results are not shown). While for higher coupling strengths, the imperfection of the chimera patterns was observed in the upper and middle rows of Fig. 6. Figures 6(a)–6(c) represent the spatiotemporal behavior of amplitude (x_i), local order parameter (L_i), and snapshot at the particular time $t = 2410$, respectively, for coupling strengths $\epsilon = 0.25$ and $g_c = 0.1$. These two spatiotemporal dynamics [Figs. 6(a) and 6(b)] suggest that the incoherent regions are not static in space and time, rather they vary erratically and we refer to them as imperfect

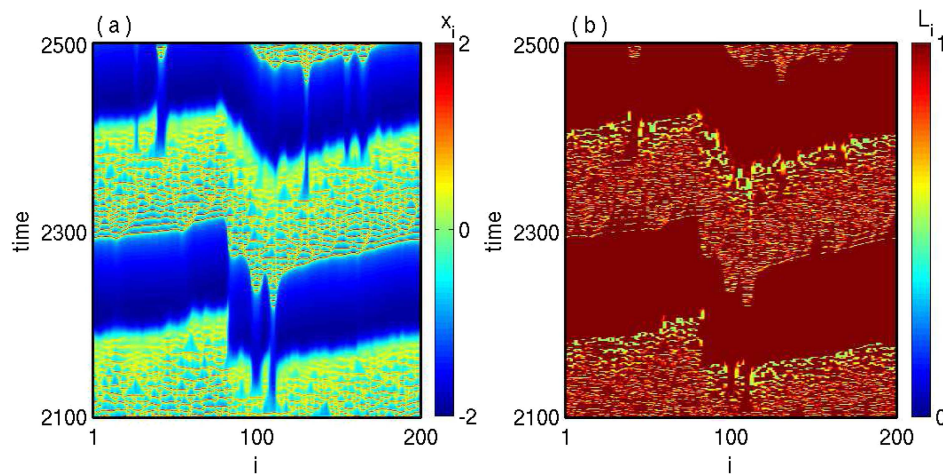


FIG. 7. Spatiotemporal plots of (a) membrane potential x_i and (b) local order parameter L_i of a hypernetwork with nonlocal chemical and local electrical synapses. Here, $R = 0.1$, $\epsilon = 0.3$, and $g_c = 0.15$.

chimera states. This imperfection decreases with increased values of the synaptic coupling strengths as $\epsilon = 1.5$, $g_c = 0.6$ [Figs. 6(d)–6(f)]. From Fig. 6(d), it is observed that the variation of the incoherent and coherent population is small compared to Fig. 6(a) and the corresponding characterization is shown in Fig. 6(e). Also, the multiplicities of the incoherent regions are lower [Fig. 6(f)] compared to Fig. 6(c), distinguished by typical snapshots of the amplitude at the particular time instant $t = 2450$. Another important observation is traveling coherent states that arise for further increased values

of the synaptic coupling strengths, $\epsilon = 4.6$ and $g_c = 1.32$ in Figs. 6(g)–6(i). The stationarity patterns from Figs. 6(g) and 6(h) show that the coherent profile is also not static, but it is shifted smoothly in space with respect to time. At two particular time instants $t = 2350$ and $t = 2400$, the snapshots are drawn in Fig. 6(i), denoted by red and magenta color, respectively. Notice that the coherent structures in Fig. 6(i) are shifted smoothly with respect to time.

Next, we study the coupled neuronal hypernetwork in which all neurons communicate through nonlocal chemical and local electrical

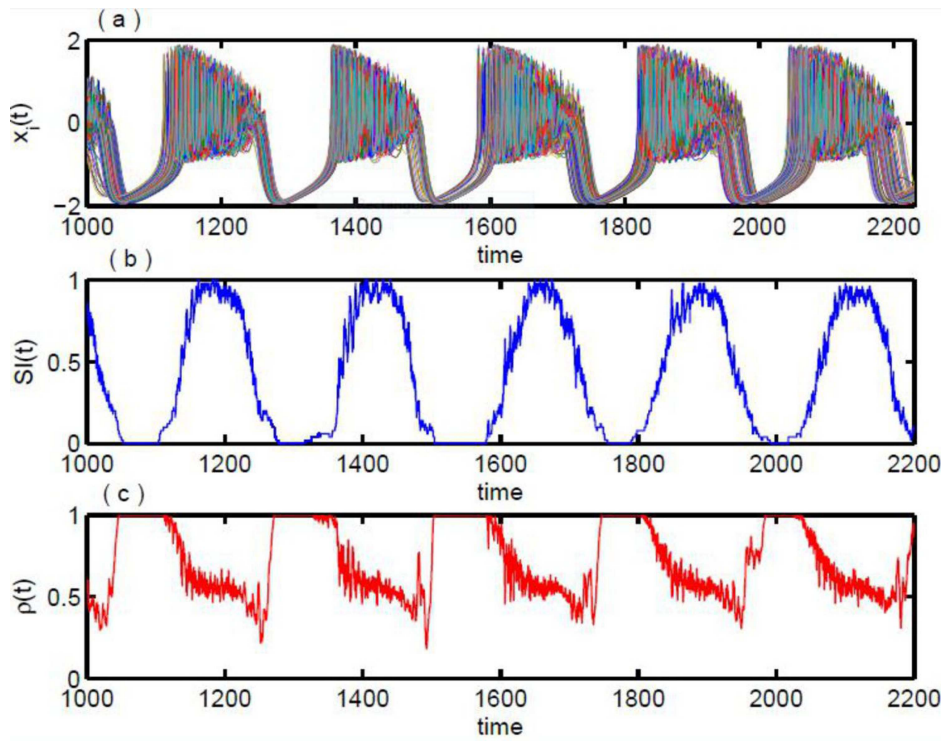


FIG. 8. Time evolution of (a) the membrane potential x_i and (b) the instantaneous strength of incoherence $S_i(t)$ and (c) global order parameter $\rho(t)$, where $\epsilon = 0.3$, $g_c = 0.15$, and $R = 0.1$.

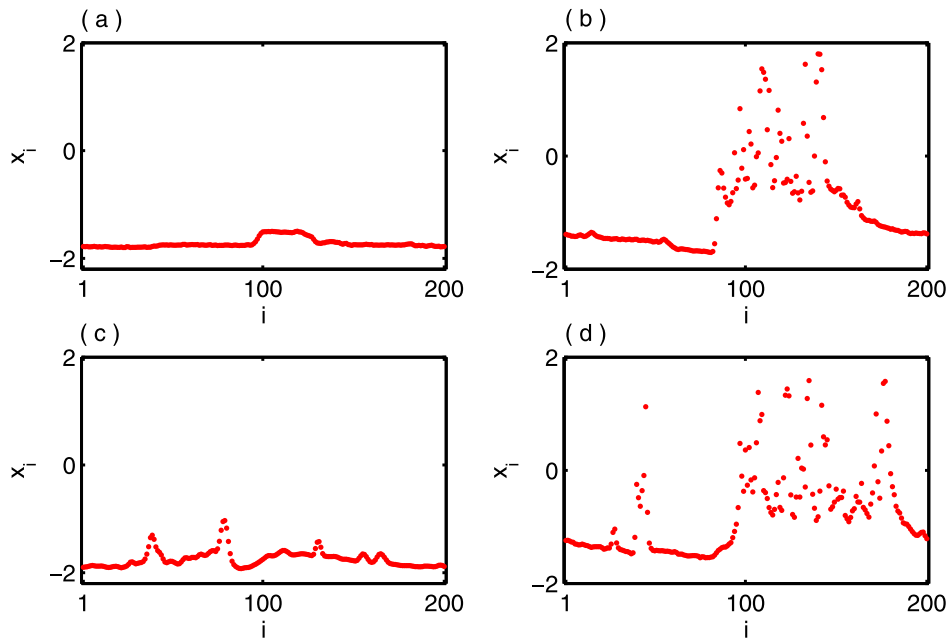


FIG. 9. Snapshot of the variable x_i at four different times (a) $t = 1550$, (b) $t = 2270$, (c) $t = 2435$, and (d) $t = 2500$. Other parameters are all the same as in Fig. 8.

synapses. Here, we observe the existence of a spike chimera state. The spatiotemporal plot in Fig. 7(a) shows that during the time period $t \in [2435, 2455]$, all the neurons are in a quiescent state, which causes phase coherence in the course of time. Figure 7(b) demonstrates the maximum coherency of the neurons in the quiescent state where

$L_i \approx 1$. The time evolution of all the neurons in the network [Eq. (1)] is plotted in Fig. 8(a). Figures 8(b) and 8(c) exhibit the variation of the instantaneous strength of incoherence $SI(t)$ and the global order parameter $\rho(t)$ with respect to time. From these figures, we clearly see that $SI(t)$ takes the value 0, whenever the quiescent states

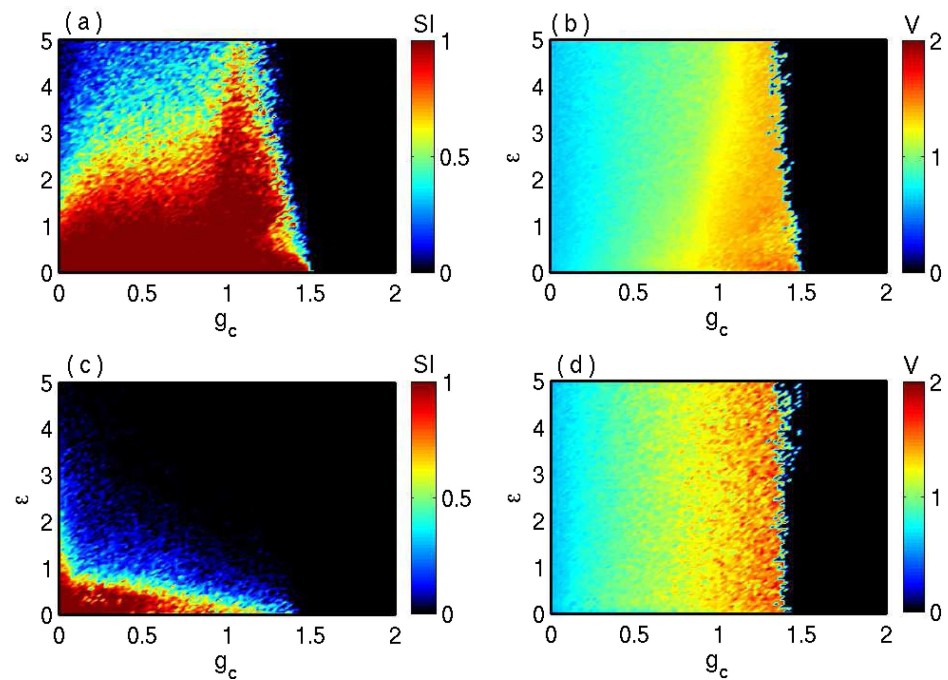
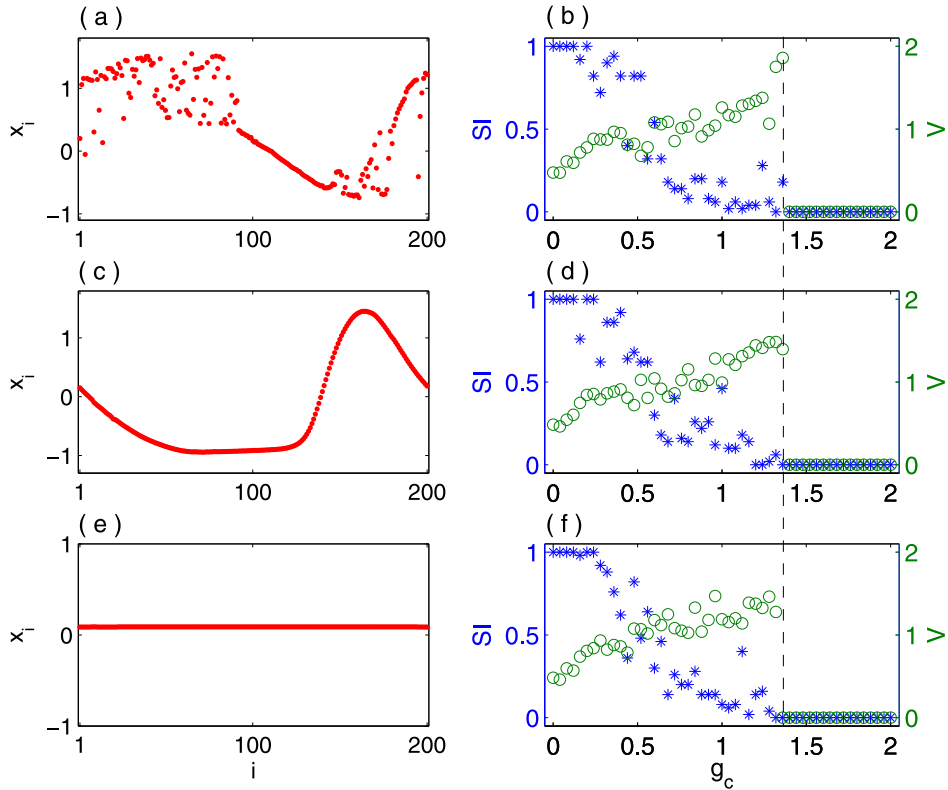


FIG. 10. The different dynamical states are characterized by SI (left column) and V (right column) in the (g_c, ϵ) parameter plane. Upper and lower rows respectively represent the results for local and nonlocal ($R = 0.1$) bidirectional electrical synapses with unidirectional chemical interactions.

occur together, for other time $SI(t) \in (0, 1)$. The same phenomenon is also manifested in Fig. 8(c) in terms of the instantaneous global order parameter $\rho(t)$. The neurons in the quiescent state are manifested with maximum coherency among them with $\rho(t) \approx 1$. For a better understanding of these scenarios, we take snapshots in terms of amplitudes of the variable $x_i(t)$ at different time instances. In the snapshot at time $t = 1550$, phase coherence due to quiescent state is shown in Fig. 9(a). Due to the appearance of few spiking and quiescent states, Fig. 9(b) exhibits the chimera state at $t = 2270$. Similarly taking another two snapshots at times $t = 2435$ and $t = 2500$, phase coherence and chimera state are observed in Figs. 9(c) and 9(d), respectively.

To characterize the different collective states and transitions among them, SI and V are calculated for local bidirectional electrical synapses in the presence of local unidirectional chemical synapses. The results are shown in Figs. 10(a) and 10(b). Figures 10(c) and 10(d) give the results for nonlocal electrical synaptic interactions. The incoherent and chimera regions in Fig. 10(a) are larger compared to those in Fig. 10(c) in the (g_c, ϵ) parameter plane, which indicates that the presence of nonlocality in the coupling configuration with unidirectional chemical synaptic mode leads to the suppression of incoherent and chimera states. The enhancement of coherent state is also observed when the chemical synaptic coupling strength increases. Also, note that for both local synaptic connections, there is a narrow region for the synchronous coherent states characterized by V, displayed in Fig. 10(b) [as black color areas are almost equal



in Figs. 10(a) and 10(b)], while the local and nonlocal combination gives rise to the appearance of synchronized coherent state with a fixed steady state region [Figs. 10(b) and 10(d)].

V. GLOBAL STABILITY OF CHIMERA STATES

Multistability, the coexistence of different stable states for a given set of parameter values, plays a crucial role in dynamical systems. In most of the neuronal systems, it is an inherent feature, which mimics different brain states operating on a particular object. So, from a neuroscientific point of view, it is very important to quantify the dynamical regimes of multistable states. In a coupled neuronal network, several types of collective dynamical states such as incoherent, chimera, and coherent states coexist due to the multistability of the entire dynamical network. In this section, we investigate the robustness of the various dynamical states against different initial conditions which are discussed in Secs. III and IV.

At first, we dredge Sec. III to investigate the multistability of incoherent, spike chimera and coherent states. Here, solely a unidirectional nonlocal chemical synaptic network is considered, where two types of coherent structures and the chimera state are strongly dependent on the initial conditions. The coexistence of chimera with the coherent states is shown in Fig. 11. For the fixed coupling radius $R = 0.25$ and synaptic strength $g_c = 1.36$, the snapshots of the amplitudes at $t = 2380$ for the chimera and two types of coherent states

FIG. 11. Coexistence of chimera and coherent states for fixed $R = 0.25$ and $g_c = 1.36$: (a) chimera, (c) synchronized coherent, and (e) global death state. Right panel shows the variation of SI and V with respect to g_c with the same initial conditions used in the left panel, where left and right y-axes show the variations of SI and V, respectively.

are plotted in Figs. 11(a), 11(c), and 11(e) by only varying the initial conditions of each oscillator. The characterizations of these states are done by plotting the values of SI and V. The blue star in the left axis of Figs. 11(b), 11(d), and 11(f) indicates the variation of SI by varying the synaptic strength g_c . Accordingly, to distinguish these two coherent states, we calculate the velocity V that is plotted with respect to g_c and denoted by the green open circle in the right axis. A dashed black line is drawn along $g_c = 1.36$, which cuts the SI value at $(0, 1)$ with a nonzero value of V in Fig. 11(b). This feature indicates the existence of a chimera state in Fig. 11(a). Again, the black line intersects the SI at "0" in Figs. 11(d) and 11(f), which refers to the appearance of coherent states in Figs. 11(c) and 11(e). The oscillatory and steady coherence dynamics are verified by the values of V that cut the dashed black line at nonzero and zero values, respectively, in Figs. 11(d) and 11(f).

To quantify these multistable states against a large number of initial conditions, we adopt a pioneer measurement as basin stability (BS), which deals with the volume of the basin of attraction. This framework is a robust gadget to quantify different multistable states and can be easily applied to even high-dimensional complex systems. It serves as a measure of the likelihood of return to a desired state after being subjected to any random perturbations and thus explains to what extent the state is stable in classical probability sense. BS is defined as

$$\text{BS} = \int_{\mathcal{B}} \chi(x)\rho(x)dx, \quad (8)$$

where \mathcal{B} be the set of possible perturbed states x , $\chi(x) = 1$ if the system converges to the synchronized state after perturbation x and 0 otherwise, and $\rho(x)$ be the density of the perturbed states with $\int_{\mathcal{B}} \rho(x)dx = 1$. For computing BS numerically, we simulate

the whole system for T sufficiently large number of different initial conditions drawn uniformly randomly from its phase space, and let the number of initial conditions that finally arrive at our desired state is Q . Then, BS for that state is calculated as $\frac{Q}{T}$, which belongs to $[0, 1]$. BS = 0 means that for any random initial condition, that state is unstable and it is globally stable for BS = 1.0, while $0 < \text{BS} < 1.0$ corresponds to the probability of getting that state for any random initial condition from its phase space. Here, we choose different initial conditions from its phase space volume $[-1.5, 2.0] \times [-7.0, 1.0] \times [2.9, 3.4]$. To explore the whole scenario of the variation of BS, we compute the phase space of (R, g_c) based on the SI and V measurements. For the range of $R \in [0.005, 0.5]$ and $g_c \in [0, 2]$ in the (R, g_c) plane, the BS for incoherent, chimera, and synchronized coherent and coherent steady state for Sec. III is plotted in Figs. 12(a)–12(d), respectively. The deep red region in the color bar takes the values "1," which means that the full basin of attraction of the coupled systems supports for the corresponding dynamical states. The black portion in the color bar is associated with the "0" value, which indicates that no initial condition from the basin volume produced that dynamical states, while mixing colors of the color bar denote the number of fraction of initial conditions for the appearance of that state. Figure 12(a) represents the BS for the incoherent state. From this figure, it is clearly shown that up to certain critical values of R and g_c , full basin support for incoherent states (for the deep red region) and after that it has strong coexistence (blue and other mixing colors) with chimera states, and further larger values of the R and g_c (black region), no initial condition from the basin volume produced incoherent states. The variation of BS for chimera states is shown in Fig. 12(b) and these have a strong coexistence with the coherent states. Figure 12(c) illustrates the BS diagram of the synchronous coherent state, which tells that in the (R, g_c) parameter space, there is an island where only

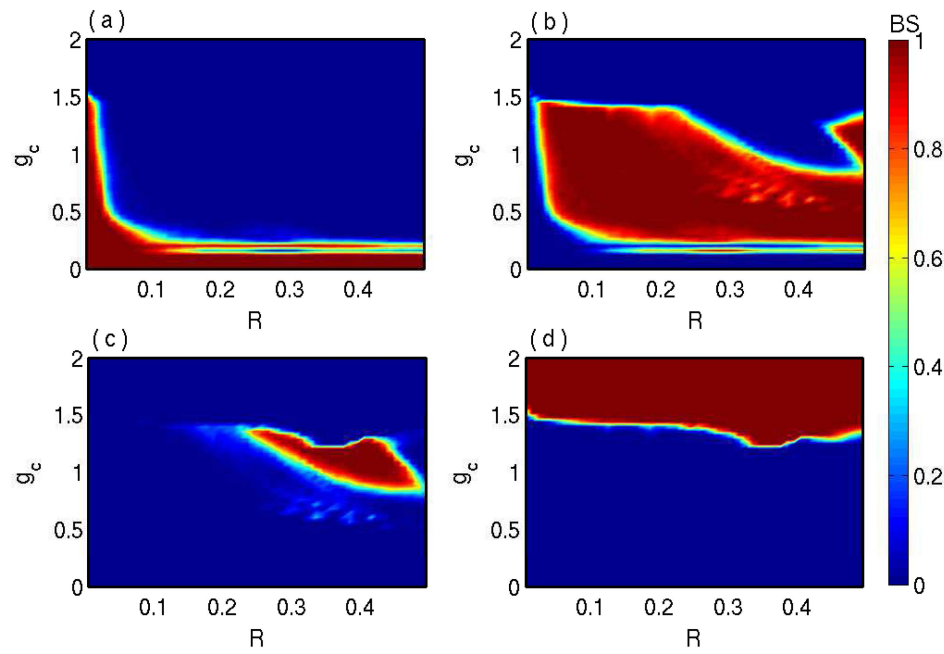


FIG. 12. BS in the (R, g_c) parameter space in the absence of electrical synapse: (a) incoherent, (b) chimera, (c) phase coherence, and (d) global death states.

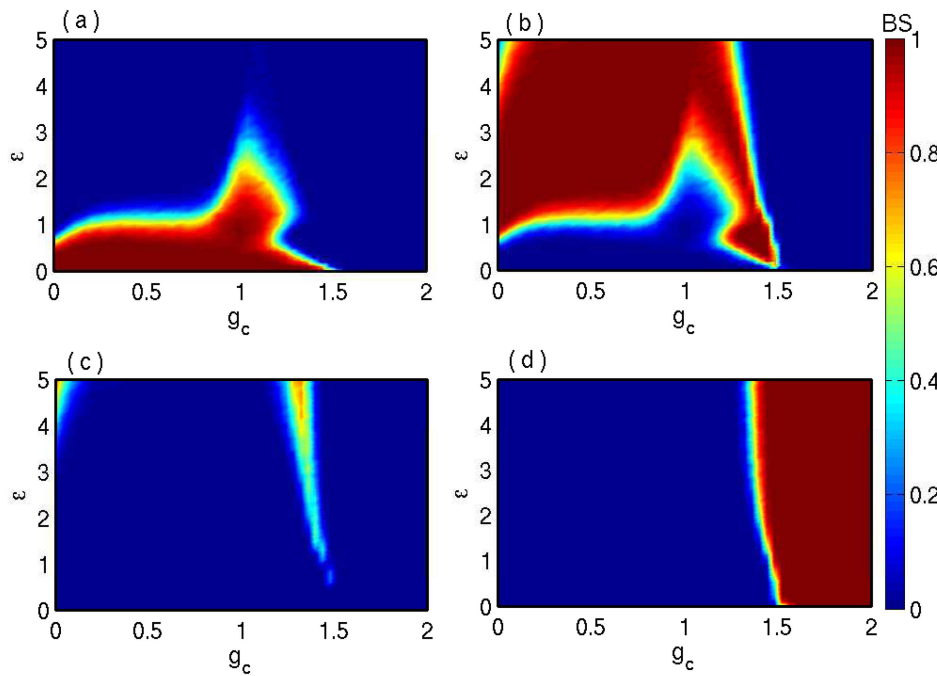


FIG. 13. BS in the (g_c, ϵ) parameter space for different dynamical states: (a) incoherent, (b) chimera, (c) synchronous coherent, and (d) coherence death states using local chemical and electrical synapses.

this state appears. For almost all values of the coupling radius, there are certain values of g_c after that nontrivial homogeneous steady state come up by Fig. 12(d).

Now, we recapitulate the results presented in Sec. IV by applying the concept of basin stability. The coexistence of chimera state with

incoherent and coherent states in the presence of local bidirectional electric synapse and local unidirectional chemical synapse is quantified by the basin stability framework in Fig. 13. The color coded [Figs. 13(a)–13(d)] represents the basin stability for incoherent, chimera, and two structurally different type of coherent states in the (g_c, ϵ)

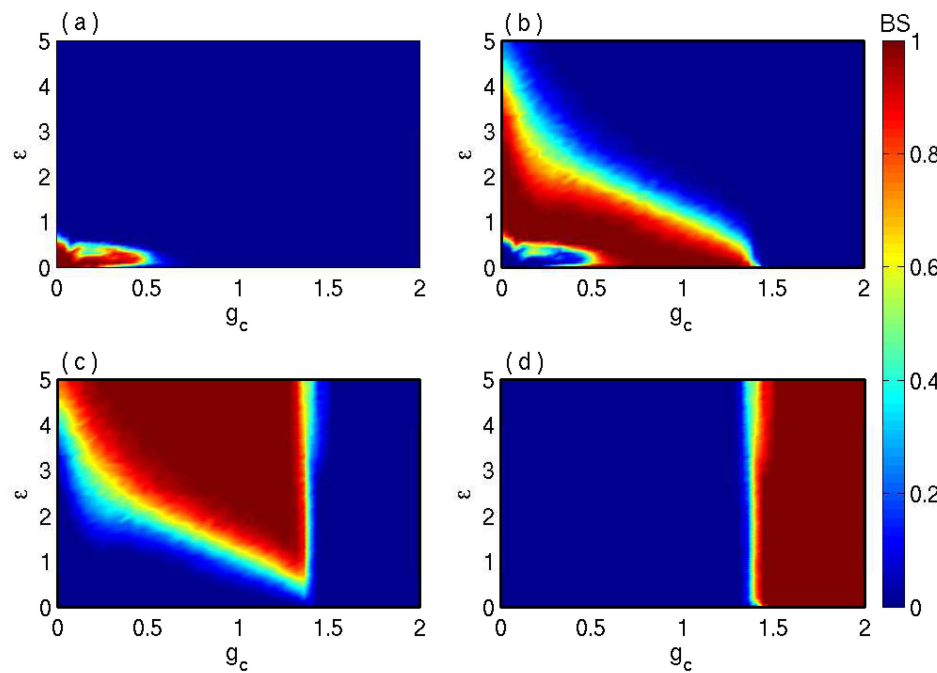


FIG. 14. Multistability of (a) incoherent, (b) chimera, (c) phase coherent, and (d) global death states are quantified in the (g_c, ϵ) plane in terms of BS for non-local unidirectional chemical ($R = 0.1$) with local bidirectional electrical coupling.

parameter space, where the color bar shows the variation of BS. Figure 13(a) shows the BS for incoherent state. It has a strong coexistence with the chimera state. For few lower values of electrical coupling strength, it is monostable; beyond that, it loses its stability. BS of the chimera state is described in Fig. 13(b). In the (ϵ, g_c) parameter space, there are few regions where it shares basin of attraction with other dynamical states, but there is a sufficient region where it is monostable. The tiny multistable region of the synchronous coherent state is shown in Fig. 13(c). The rapid transition of the stability of the death state is delineated in Fig. 13(d), although it enhances gradually by increasing ϵ .

Similarly, the quantification of such states for local electrical and nonlocal chemical interactions is displayed in Fig. 14, where the coupling radius for chemical coupling is $R = 0.1$. The BS measure of the incoherent state is drawn in Fig. 14(a). By introducing any of the synaptic coupling strengths, the BS of this incoherent state promptly decreases from 1 and it becomes unstable swiftly. Here, the chimera state swallows the basin of attraction of the incoherent state, as the conclusion of Fig. 14(b). By increasing either or both the coupling strengths with an appropriate amount, the chimera state can be able to exploit the whole phase space and becomes monostable. Beyond increasing the synaptic coupling strengths, it misses out its stability, and the BS of the synchronous coherent state gradually increases. Here, the chimera state [Fig. 14(b)] strongly coexists with synchronized [Fig. 14(c)] and incoherent states [Fig. 14(a)]. The synchronous coherent state remains monostable up to $g_c = 1.3$; after that, the coherent steady state swallow its basin of attraction swiftly, as shown in Fig. 14(d). For almost every value of ϵ , its transition point is the same, but for higher values of ϵ , there is a small region where it coexists with a synchronous coherent state. Such a strong coexistence appears due to the combined effect of local and nonlocal coupling interactions.

VI. FIRING REGULARITY

Next, we investigate the firing regularity of the spike train of the individual neurons in the neuronal network (1) by calculating two quantities, namely, interspike interval (ISI) and the corresponding coefficient of variation (CV). The distribution of ISI represents the time lapse between two consecutive spikes in a sufficient long spike sequence, while CV signifies the variation of the regularity in the firing pattern. It is known that the spike timing of neurons is extremely irregular due to the presence of successive stochastic forces. This reflects a random process where the relationship between spikes and stimulus is stochastic. An instantaneous estimate of the spike rate of a neuronal network can be obtained by averaging the responses of individual neurons and a random process can be used to model them.³⁸

Now, the spikes are discrete events, so the probability distribution of interspike intervals should be discrete. Neuroscientists already observed that the generation of each spike occurs randomly with no memory for the last occurrence but depends on the underlying driving signal, which is continuous or analog, known as the instantaneous firing rate. Hence, it may be referred to as the independent spike hypothesis—a sort of “null hypothesis.” Then, the spike train would be described as a particular notion of a random process known as Poisson process. For a known average rate, the Poisson distribution

gives the probability of a given number of spikes within a refractory period. For most of the neuronal systems, the spike rates are small enough; it rarely generates in the whole span time. So, Poisson distribution is an appropriate description of the spiking neurons. Most of the neuronal spiking can be truly Poisson process, but certain features of neuronal firing may violate the independent spike hypothesis.³⁹ Following the generation of an action potential, there is an interval of time, known as the absolute refractory period during which the neuron cannot fire another spike. For a longer interval known as the relative refractory period and during this period, the likelihood of a spike being fired is much reduced. Bursting is the common feature of neuronal spiking patterns, where its activity deviates a lot from Poisson. Some neurons generate action potentials in clusters or bursts form, and these tend to be poorly described by a Poisson spike-generation process.⁴⁰

Let the distribution of ISI of the i th neuron be $F_i(x)$, where $\int_{t_0}^{t_0+s} F_i(x) dx$ represents the probability of occurrence of the next spike of the i th neuron in the interval $[t_0, t_0 + s]$, given that the last spike occurred at time t_0 . Then, the mean firing interval of the i th neuron is denoted by $\langle s_i \rangle$ and defined as

$$\langle s_i \rangle = \int_0^\infty x F_i(x) dx. \quad (9)$$

In the theory of probability, CV is a standardized measure of dispersion of a probability distribution. The distribution of interspike intervals derived from a spike train under stationary conditions is sharply peaked. To quantify the width of the interval distribution, neuroscientists often evaluate the CV as the ratio of the standard deviation and the mean. The CV_i of the i th neuron quantifies the width of the interval distribution, which is defined as

$$CV_i = \frac{\sqrt{\int_0^\infty x^2 F_i(x) dx - \langle s_i \rangle^2}}{\langle s_i \rangle}. \quad (10)$$

For numerical computation, the mean firing interval of the i th neuron is estimated as $\langle s_i \rangle = \frac{1}{M_i} \sum_{j=1}^{M_i} (t_{j+1} - t_j)$ and the mean-square deviation of ISIs as $\frac{1}{M_i} \sum_{j=1}^{M_i} (t_{j+1} - t_j)^2$, where t_j is the time of the j th spike and M_i is the total number of spikes in the spike sequence of the i th neuron during the long time period. So,

$$CV_i = \frac{\sqrt{\frac{1}{M_i} \sum_{j=1}^{M_i} (t_{j+1} - t_j)^2 - \langle s_i \rangle^2}}{\langle s_i \rangle}. \quad (11)$$

The mean ISI and CV of the whole network are estimated as $\langle s \rangle = \frac{1}{N} \sum_{i=1}^N \langle s_i \rangle$ and $CV = \frac{1}{N} \sum_{i=1}^N CV_i$. If $CV = 1$, then the spike train of the entire network will follow a Poissonlike process, while a more regular firing pattern yields CV less than 1. $CV = 0$ represents that each neuron of the network fires periodically. $CV > 1$ implies that the spike train is less regular compared to the Poissonlike process with the same firing rate.⁴¹ So, CV indicates the deviation of the spike sequence from a random Poisson process. As much as $CV < 1$, it corresponds the higher firing regularity and more ordered spiking pattern in the entire network.

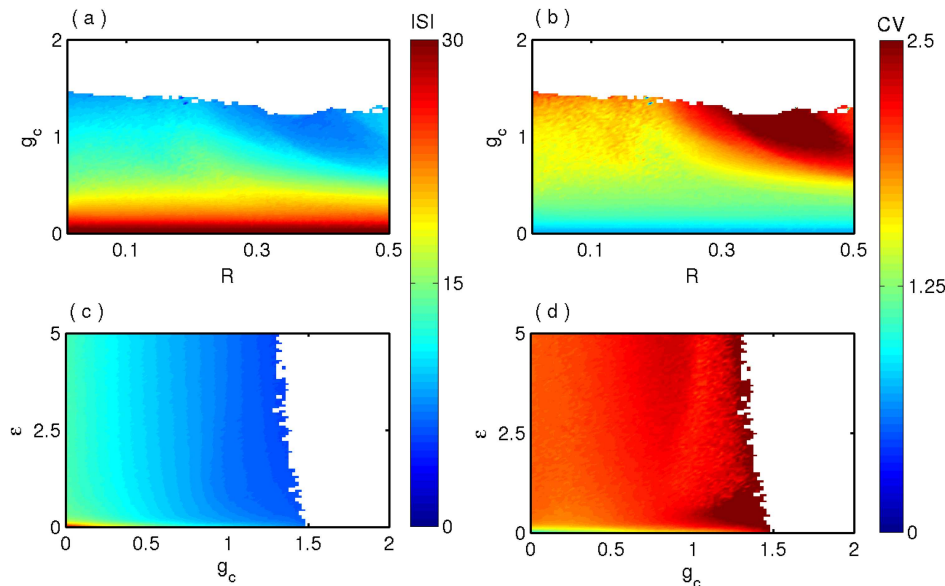


FIG. 15. Color bars indicate the variation of ISI (left panel) and CV (right panel) for different parameter plane. (a) Variation of ISI and (b) corresponding CV for one way nonlocally coupled HR neurons in the (R, g_c) phase diagram. (c) Variation of ISI and (d) corresponding CV for hyperneuronal network, i.e., presence of local electrical ring with nonlocal chemical interaction (lower panel, $R = 0.1$) in (g_c, ϵ) parameter space.

We again dredge Sec. III to gauge the firing patterns of the neurons for different dynamical states in the sole presence of a unidirectional chemical neuronal network [i.e., for $\epsilon = 0.0$ in Eq. (1)]. For this monolayer neuronal network, the mean ISI and CV are drawn in Figs. 15(a) and 15(b), respectively. From the ISI variation against two tuning parameters R and g_c , we find that the mean ISI is larger for the incoherent state and decreases with increasing the chemical synaptic coupling strength g_c . However, for the synchronous coherent states (corresponding to Fig. 5), the time interval between two consecutive firings becomes small. So, the coherent dynamics promotes the entire neuronal network to frequent firing. Up to a certain threshold of g_c , ISI values remain finite; after that, all the neurons go to steady state dynamics (resting patterns), where mathematically, their ISI values will be infinite, represented by the white region in Fig. 15(a). To understand the regularity of firing pattern of the spike train, we plot CV in Fig. 15(b). The spike train is more regular for the incoherent states as $CV < 1$, and as g_c increases, it becomes less regular than a Poisson process. Finally, for the synchronous coherent states, $CV > 1$, which implies that the spike train is less regular than a Poisson process with almost identical firing rate. Next we simulate the firing regularity corresponding to Sec. IV, in the presence of both types of synaptic interactions, for two different values of chemical coupling radius. Here, the neurons communicate through local bidirectional electrical synapses and nonlocal unidirectional chemical synapses. Figures 15(c) and 15(d) represent the variation of ISI and CV in the (g_c, ϵ) parameter plane with a fixed value of coupling radius $R = 0.1$. From this picture, it is concluded that the presence of the local bidirectional electrical gap junctional interactions does not generate significant changes in the firing regularity of the spike train of all the neurons in the neuronal hypernetwork, which means that only chemical synaptic interactions determine various firing regularity patterns in the spike train.

VII. CONCLUSION

We have investigated the emergence and existence of nonstationary chimera states in a neuronal network by taking the Hindmarsh–Rose neuronal oscillator as local dynamics of each node. First, we have observed a new phenomenon, the spike chimera state in nonlocally unidirectional chemical synaptic interaction network and this type of chimera state is quite different from the classical chimera states. Previous studies on nonstationary chimera states (like breathing chimera,⁴² alternating chimera,⁴³ imperfect chimera²²) where the chimera states persist in the whole time span, i.e., in each time, the snapshot shows coexistence of coherent and incoherent subpopulations. However, in our case, for the first time, we observed that the spike chimera state does not persist for the whole time span. There is some intermediate time interval where the fully coherent state emerges due to the combined appearance of the quiescent state of all the neurons in the coupled neuronal network. Previously, it was found that chimera states are chaotic transient,⁴⁴ which means after a sufficiently long time, chimera states suddenly disappear and eventually collapse to the coherent motions. Here, our found spiking chimera patterns show an alternation over times due to the presence of the multitempore features in the neuronal systems. By rigorous spatiotemporal plots, instantaneous strength of incoherence, and the order parameter characterization, we established the occurrence of such chimera state in a wide range of different parameter spaces. The average strength of incoherence is used to distinguish between incoherent, chimera, and coherent states. Next, we explored the emergence of chimera states in the presence of both electrical and chemical synapses. It was observed that the combined effect of these two types of synapses with local interaction leads to the emergence of imperfect traveling chimera states and traveling coherent motion. The spike chimera state is also observed for unidirectional (nonlocal) chemical and local electrical synapses. From the above

two cases, one can conclude that the presence of unidirectional non-local chemical synapse plays an important role for the emergence of spike chimera states. For the spike chimera state, the simultaneous coexistence of coherent and incoherent subpopulation emerges and annihilates serially one after another. We have checked that this successive alternation persists for a long time span.

In addition, we observed that the chimera state together with other dynamical states (incoherent, synchronized coherent, and amplitude death) has a strong coexistence with respect to the initial conditions. To quantify them, we have used a global stability framework, namely, the basin stability measurement, which interplays with the large number of initial conditions from the basin volume. Finally, we have estimated the time interval between two consecutive firings of neurons by calculating the interspike interval, and the corresponding firing regularity of the spike trains was characterized through the coefficient of variation measurement. Our investigations may help one to better understand the neuronal synchrony and desynchrony patterns in regard to several neuronal processes. Spike synchrony is a fundamental feature in the various neuronal processes. This synchrony may break down for certain external perturbation and lead to the coexistence of synchronous and asynchronous neuronal oscillations (resemblance of chimera features). In this context, the estimation of the CV and ISI on the spike chimera may assist to control the undesired neuronal oscillations.

ACKNOWLEDGMENTS

D.G. was supported by the Department of Science and Technology, Government of India (Project No. EMR/2016/001039).

REFERENCES

- ¹F. A. C. Azevedo, L. R. B. Carvalho, L. T. Grinberg, J. M. Farfel, R. E. L. Ferretti, R. E. P. Leite, W. J. Filho, R. Lent, and S. H. Houzel, *J. Comput. Neurosci.* **51**, 532 (2009).
- ²E. R. Kandel, J. H. Schwartz, and T. M. Jessell, *Principles of Neural Science* (McGraw Hill Education, 2000), ISBN: 0-8385-7701-6.
- ³A. E. Pereda, *Nat. Rev.* **15**, 250 (2014).
- ⁴S. G. Hormuzdi, M. A. Filippov, G. Mitropoulou, H. Monyer, and R. Bruzzone, *Biochim. Biophys. Acta* **1662**, 113 (2004).
- ⁵F. Sorrentino, *New J. Phys.* **14**, 033035 (2012).
- ⁶S. Rakshit, B. K. Bera, D. Ghosh, and S. Sinha, *Phys. Rev. E* **97**, 052304 (2018); S. Rakshit, B. K. Bera, and D. Ghosh, *Phys. Rev. E* **98**, 032305 (2018).
- ⁷C. M. Gray, P. Koenig, A. K. Engel, and W. Singer, *Nature* **338**, 334 (1989).
- ⁸M. Steriade and R. R. Llinás, *Physiol. Rev.* **68**, 649 (1988).
- ⁹J. Larson and G. Lynch, *Science* **232**, 985 (1986).
- ¹⁰Y. Kuramoto and D. Battogtokh, *Nonlinear Phenom. Complex Syst.* **5**, 380–385 (2002).
- ¹¹D. M. Abrams and S. H. Strogatz, *Phys. Rev. Lett.* **93**, 174102 (2004).
- ¹²C. R. Laing, *Physica D* **240**, 1960 (2011).
- ¹³N. C. Rattenborg, C. J. Amlaner, and S. L. Lima, *Neurosci. Biobehav. Rev.* **24**, 817 (2000).
- ¹⁴N. C. Rattenborg, *Naturwissenschaften* **93**, 413 (2006).
- ¹⁵M. J. Panaggio and D. M. Abrams, *Nonlinearity* **28**, R67 (2015); B. K. Bera, S. Majhi, D. Ghosh, and M. Perc, *Europhys. Lett.* **118**, 10001 (2017).
- ¹⁶T. Banerjee, P. S. Dutta, A. Zakharova, and E. Schöll, *Phys. Rev. E* **94**, 032206 (2016); S. Kundu, S. Majhi, P. Muruganandam, and D. Ghosh, *Eur. Phys. J. Spec. Top.* **227**, 983 (2018).
- ¹⁷M. R. Tinsley, S. Nkomo, and K. Showalter, *Nat. Phys.* **8**, 662 (2012).
- ¹⁸S. Nkomo, M. R. Tinsley, and K. Showalter, *Phys. Rev. Lett.* **110**, 244102 (2012).
- ¹⁹A. Hagerstrom, T. E. Murphy, R. Roy, P. Hövel, I. Omelchenko, and E. Schöll, *Nat. Phys.* **8**, 658 (2012).
- ²⁰B. K. Bera, D. Ghosh, and M. Lakshmanan, *Phys. Rev. E* **93**, 012205 (2016).
- ²¹B. K. Bera and D. Ghosh, *Phys. Rev. E* **93**, 052223 (2016); S. Majhi, B. K. Bera, D. Ghosh, and M. Perc, “Chimera states in neuronal networks: A review,” *Phys. Life Rev.* (published online).
- ²²B. K. Bera, D. Ghosh, and T. Banerjee, *Phys. Rev. E* **94**, 012215 (2016).
- ²³S. Kundu, S. Majhi, B. K. Bera, D. Ghosh, and M. Lakshmanan, *Phys. Rev. E* **97**, 022201 (2018); S. Kundu, B. K. Bera, D. Ghosh, and M. Lakshmanan, *Phys. Rev. E* **99**, 022204 (2019); B. K. Bera, D. Ghosh, P. Parmananda, G. V. Osipov, and S. K. Dana, *Chaos* **27**, 073108 (2017).
- ²⁴C. R. Laing, *Phys. Rev. E* **92**, 050904(R) (2015).
- ²⁵A. Yeldesbay, A. Pikovsky, and M. Rosenblum, *Phys. Rev. Lett.* **112**, 144103 (2014).
- ²⁶Y. Zhu, Z. Zheng, and J. Yang, *Phys. Rev. E* **89**, 022914 (2014).
- ²⁷V. V. Makarov, S. Kundu, D. V. Kirsanov, N. S. Frolov, V. A. Maksimenko, D. Ghosh, S. K. Dana, and A. E. Hramov, *Commun. Nonlinear Sci. Numer. Simul.* **71**, 118 (2019).
- ²⁸J. Hizanidis, N. E. Kouvaris, G. Zamora-López, A. Diaz-Guilera, and C. G. Antonopoulos, *Sci. Rep.* **6**, 19845 (2016).
- ²⁹S. Ghosh, A. Kumar, A. Zakharova, and S. Jalan, *Europhys. Lett.* **115**, 60005 (2016); S. Majhi, M. Perc, and D. Ghosh, *Sci. Rep.* **6**, 39033 (2016); V. A. Maksimenko, M. V. Goremyko, V. V. Makarov, A. E. Hramov, D. Ghosh, B. K. Bera, and S. K. Dana, *Bull. Russ. Acad. Sci. Phys.* **81**, 110 (2017); S. Majhi, M. Perc, and D. Ghosh, *Chaos* **27**, 073109 (2017); M. V. Goremyko, V. A. Maksimenko, V. V. Makarov, D. Ghosh, B. Bera, S. K. Dana, and A. E. Hramov, *Tech. Phys. Lett.* **43**, 712 (2017); V. A. Maksimenko, V. V. Makarov, B. K. Bera, D. Ghosh, S. K. Dana, M. V. Goremyko, N. S. Frolov, A. A. Koronovskii, and A. E. Hramov, *Phys. Rev. E* **94**, 052205 (2016).
- ³⁰S. Ghosh and S. Jalan, *Chaos* **28**, 071103 (2018).
- ³¹S. Jalan, S. Ghosh, and B. Patra, *Chaos* **27**, 101104 (2017).
- ³²J. Hizanidis, V. G. Kanas, A. Bezerianos, and T. Bountis, *Int. J. Bifurcat. Chaos* **24**, 1450030 (2014).
- ³³I. Omelchenko, O. E. Omel'chenko, P. Hövel, and E. Schöll, *Phys. Rev. Lett.* **110**, 224101 (2013).
- ³⁴R. Gopal, V. Chandrasekar, A. Venkatesan, and M. Lakshmanan, *Phys. Rev. E* **89**, 052914 (2014).
- ³⁵P. J. Menck, J. Heitzig, N. Marwan, and J. Kurths, *Nat. Phys.* **9**, 89 (2013).
- ³⁶S. Rakshit, B. K. Bera, M. Perc, and D. Ghosh, *Sci. Rep.* **7**, 2412 (2017); S. Rakshit, B. K. Bera, S. Majhi, C. Hens, and D. Ghosh, *Sci. Rep.* **7**, 45909 (2017); S. Rakshit, S. Majhi, B. K. Bera, S. Sinha, and D. Ghosh, *Phys. Rev. E* **96**, 062308 (2017).
- ³⁷P. Jaros, Y. Maistrenko, and T. Kapitaniak, *Phys. Rev. E* **91**, 022907 (2015).
- ³⁸P. Dayan, and L. Abbott, *Theoretical Neuroscience* (MIT Press, 2001), Chap. 1.4.
- ³⁹B. B. Averbeck, *Neuron* **62**, 310 (2009).
- ⁴⁰D. Heeger, *Poisson Model of Spike Generation* (Handout) (University of Stanford, 2000), Vol. 5.
- ⁴¹W. Gerstner, W. M. Kistler, R. Naud, and L. Paninski, *Neuronal Dynamics* (Cambridge University Press, 2014), Chap. 7.3.
- ⁴²D. M. Abrams, R. Miroollo, S. H. Strogatz, and D. A. Wiley, *Phys. Rev. Lett.* **101**, 084103 (2008).
- ⁴³S. Majhi and D. Ghosh, *Chaos* **28**, 083113 (2018).
- ⁴⁴M. Wolfrum and O. E. Omel'chenko, *Phys. Rev. E* **84**, 015201(R) (2011); F. P. Kemeth, S. W. Haugland, L. Schmidt, I. G. Kevrekidis, and K. Krischer, *Chaos* **26**, 094815 (2016).